Published in final edited form as:
IEEE Trans Neural Syst Rehabil Eng. 2011 October ; 19(5): 501–513. doi:10.1109/TNSRE.2011.2163145.

Limb-state information encoded by peripheral and central somatosensory neurons: Implications for an afferent interface

Douglas J. Weber [Member, IEEE],
Department of Physical Medicine and Rehabilitation and the Department of Bioengineering, University of Pittsburgh, Pittsburgh, PA, 15213, USA, phone: 412-624-4055;

Brian M. London [Student Member, IEEE],
Department of Physiology, Feinberg School of Medicine, Northwestern University, 303 E. Chicago Ave., Chicago, IL 60611, USA

James A. Hokanson [Student Member, IEEE],
Department of Bioengineering, University of Pittsburgh, Pittsburgh, PA, 15213, USA

Christopher A. Ayers,
Department of Bioengineering, University of Pittsburgh, Pittsburgh, PA, 15213, USA

Robert A. Gaunt [Member, IEEE],
Department of Physical Medicine and Rehabilitation and the Department of Bioengineering, University of Pittsburgh, Pittsburgh, PA, 15213, USA

Ricardo R. Torres,
Department of Physiology, Feinberg School of Medicine, Northwestern University, 303 E. Chicago Ave., Chicago, IL 60611, USA

Boubker Zaaimi, and
Department of Physiology, Feinberg School of Medicine, Northwestern University, 303 E. Chicago Ave., Chicago, IL 60611, USA

Lee E. Miller [Member, IEEE]
Departments of Physiology and Physical Medicine and Rehabilitation, Feinberg School of Medicine, and the Department of Biomedical Engineering, Northwestern University, 303 E. Chicago Ave., Chicago, IL 60611, USA

Douglas J. Weber: weber.doug@gmail.com; Brian M. London: blondon@u.northwestern.edu; James A. Hokanson: jim.hokanson@gmail.com; Christopher A. Ayers: chris.ayers@gmail.com; Robert A. Gaunt: rag53@pitt.edu; Ricardo R. Torres: ricardort@gmail.com; Boubker Zaaimi: boubkerz@gmail.com; Lee E. Miller: lm@northwestern.edu

Abstract

A major issue to be addressed in the development of neural interfaces for prosthetic control is the need for somatosensory feedback. Here, we investigate two possible strategies: electrical stimulation of either dorsal root ganglia (DRG) or primary somatosensory cortex (S1). In each approach, we must determine a model that reflects the representation of limb state in terms of neural discharge. This model can then be used to design stimuli that artificially activate the nervous system to convey information about limb state to the subject. Electrically activating DRG neurons using naturalistic stimulus patterns, modeled on recordings made during passive limb movement, evoked activity in S1 that was similar to that of the original movement. We also found that S1 neural populations could accurately discriminate different patterns of DRG stimulation across a wide range of stimulus pulse-rates. In studying the neural coding of limb-state in S1, we also decoded the kinematics of active limb movement using multi-electrode recordings in the monkey. Neurons having both proprioceptive and cutaneous receptive fields contributed equally to this decoding. Some neurons were most informative of limb state in the recent past, but many others appeared to signal upcoming movements suggesting that they also were modulated by an

efference copy signal. Finally, we show that a monkey was able to detect stimulation through a large percentage of electrodes implanted in area 2. We discuss the design of appropriate stimulus paradigms for conveying time-varying limb state information, and the relative merits and limitations of central and peripheral approaches.

Index Terms

dorsal root ganglia; multi-electrode array; neural coding; neural prostheses; sensory cortex; sensory feedback

I. Introduction

The recent development of state of the art prosthetic devices such as the i-Limb (Touch Bionics, Inc.) and the Deka Arm (Deka Research and Development Corp.) demonstrate that the technology for powered prostheses is advancing at a high rate. However, body-powered systems are still preferred by many users, in large part because of the proprioceptive feedback provided by the control cable, which directly links the end point force, position and velocity of an intact anatomical joint to the prosthetic joint controlled by the cable [1]. This observation is consistent with the fact that patients lacking proprioceptive feedback due to large-fiber neuropathy and other causes suffer from greatly impoverished movement quality, despite having normal muscle strength [2]. The importance of somatosensory feedback prompts the need for an afferent interface to parallel the efferent interfaces that have been under development for over a decade [3–8]. The afferent interface would provide users with both tactile and proprioceptive information from an artificial or paralyzed limb.

In this manuscript, we describe experiments that explore two complementary approaches to the goal of providing meaningful artificial somatosensory input to a user through electrical stimulation of the nervous system. One approach is to use intracortical microstimulation (ICMS) based on the natural patterns of activity recorded within the primary somatosensory cortex (S1) of awake monkeys. The other approach relies on primary afferent microstimulation (PAMS) in the dorsal root ganglia, which we have investigated in anesthetized cats. In both studies, we examined associations between neural firing rates and limb kinematic variables to gain some initial insight into how we might encode these state variables in multichannel microstimulation patterns. These studies also demonstrate two different approaches for evaluating performance of a somatosensory afferent interface. In the PAMS studies, we used multichannel neural recordings to measure signals conveyed to S1 by various patterns of DRG stimulation. In the ICMS studies, we use behavioral tasks to evaluate both the detectability and discriminability of ICMS patterns delivered to area 2 of S1 in monkeys.

Selective stimulation of first order (i.e. primary) muscle and cutaneous afferent neurons in the peripheral nerve or spinal roots may represent the simplest approach for developing an afferent interface in cases where portions of the peripheral nerves and spinal cord remain intact. The basic feasibility has already been demonstrated in a limited number of human studies [9–13]. PAMS could be implemented by implanting microelectrode arrays in the DRG, where fibers from a range of sensory modalities can be recruited selectively at low (1 – 5 μA) stimulation intensities [14]. Since the majority of primary afferent neurons from an entire limb are grouped into ~2–4 adjacent segments, the DRG provide a compact target for accessing a large set of primary afferent neurons for the limb.

A second approach to providing somatosensory information to the central nervous systems is to stimulate the cortex directly. By implanting multi-electrode arrays in S1, it may be

possible to evoke useful somatosensory perceptions by ICMS. The primary visual cortex (V1) has been the focus of considerable development work toward an ICMS-based visual prosthesis. Humans that have been implanted with stimulating electrodes in V1 are able to detect small spots of light (phosphenes) of differing size, color, and location [15]. Systematic psychophysical testing indicated that monkeys with chronic V1 implants were able to use electrically induced phosphenes to perform a memory saccade task [16].

Our initial results demonstrate that both DRG and S1 may provide the neural substrate necessary to create an afferent interface for transmitting limb-state information into the nervous system. In this paper we describe these results, compare the relative merits of each approach, and highlight key challenges facing the development of a highly functional afferent interface for providing somatosensory feedback.

II. Methods

Primary afferent microstimulation (PAMS) and cortical recording studies were performed in four anesthetized cats under protocols approved by the University of Pittsburgh IACUC. Cortical recording and stimulation studies were performed in four behaving monkeys (A, T, M, and P) under protocols approved by the Northwestern University IACUC.

A. S1 neuronal responses to PAMS in anesthetized cats

1) Experimental setup—We performed two groups of experiments to examine variations in S1 neuronal responses elicited by different patterns of PAMS. We used charge-balanced stimulation pulses with a 200 μs cathodal phase followed by a 400 μs anodal phase at half amplitude. All stimulation was monopolar with respect to a large return electrode placed in the epidural space under the vertebrae. Stimulation was performed using MS-16 stimulators (Tucker Davis Technologies, Inc, USA).

We refer to the first group of experiments as the replay pattern group, wherein the PAMS patterns were intended to mimic a natural pattern of sensory input, such as that produced during motion of the leg. We began these experiments by recording S1 and DRG neuronal spiking activity during passive movements of the hindlimb generated by a robot attached to the cat's foot (see figure 1A). Next, we created a multichannel stimulation pattern based on the DRG spiking activity recorded on either 15 (cat 1) or 30 (cat 4) DRG electrodes (see Figure 1B). We compared the S1 neural responses evoked by the replay stimulation pattern to those evoked during the passive movement. Our goal for these experiments was to determine the extent to which PAMS can evoke patterns of neural activity in S1 that are similar to those evoked during actual leg movements

In the second group of PAMS experiments, referred to as fabricated pattern trials, we systematically varied the intensity, pulse-rate, and location of PAMS inputs while measuring the neural responses in S1 (see Figure 1C). Each stimulus pattern consisted of a 500 ms train of pulses applied to a pair of DRG electrodes, followed by a 1–2 second period without stimulation. The same pattern of monopolar stimulation was applied synchronously to each electrode in the electrode pair. A large set of PAMS patterns were fabricated by varying the stimulus location (i.e. specific pairs of active electrodes in the DRG array), amplitude of stimulus current (3 – 20 μA), and pulse rate (20 – 1000 pulses per second; pps). We used pattern classifier methods to quantify the discriminability of the S1 neural response evoked by different patterns of stimulation.

2) Surgical procedures—The cat's head was supported by a stereotaxic frame and a second custom frame supported the torso, spine, and pelvis while allowing the hindlimb to move freely through its full range of motion. All surgical and experimental procedures were

performed under isoflurane anesthesia (1–2%). Blood pressure, core body temperature, respiration rate, end tidal CO_2, and oxygen saturation were measured continuously and maintained within normal, physiological ranges.

We inserted arrays of microelectrodes to a depth of 1.0 – 1.5 mm in the hindlimb region of S1, ~1 mm caudal to the cruciate sulcus and ~2 mm lateral to the midline fissure [17]. A 16-channel array (TDT, Alachua, FL) was used in cat 1, a 5×10 channel array (Blackrock Microsystems, Salt Lake City, UT) was used in cats 2 and 4, and 5×10 and 4×10 arrays (Blackrock) were inserted side by side in cat 3. We confirmed electrode placements in the hindlimb region by recording S1 neuronal responses evoked by electrical stimulation of the contralateral sciatic nerve via a bipolar nerve cuff electrode.

DRG were exposed by laminectomy as described in [18]. In cat 1, we used an array of 16 tungsten microelectrodes (each 50 μm dia.; impedance ~50 kOhms at 1000 Hz) inserted into the L7 DRG. In cats 2–4, 4×10 and 5×10 arrays of sputtered iridium oxide (SIROx) microelectrodes (Blackrock) were inserted into L6 and L7 respectively. Typical impedance values for the SIROx electrodes were ~50 kOhms at 1000 Hz.

3) Data collection—Neuronal spiking data were sampled at 25 kHz using a multichannel neural recording system (RZ2, TDT) and digitally band-pass filtered between 300 and 3000 Hz. Thresholds were determined manually for each channel and spike events were defined whenever the signal exceeded this threshold. For cat 3, the neural data were separately band passed filtered between 1 and 300 Hz to examine local field potentials (LFPs). Hindlimb kinematics were recorded with high speed motion capture systems (Vicon 460, Vicon, USA or IMPULSE, Phasespace, USA) using markers placed on the iliac crest (IC), hip, knee, ankle, and metatarsophalangeal (MTP) joints. A robotic arm (VS6556E, DENSO Robotics, USA) was used to generate center-out-and-back displacements of the left foot in the parasagittal plane.

4) Data analysis—Firing rates were computed by convolving spike times with a non-causal Gaussian kernel and sampled at 32 (passive movement and replay) or 10 (fabricated stimulation) ms intervals. With the exception of the replay analysis, firing rates were computed on unsorted multi-unit responses. LFP data was notch filtered between 55 and 65 Hz, band pass filtered between 20 and 200 Hz, and rectified.

We used multivariate linear regression to examine how well the limb kinematic variables were encoded in the firing rates of individual DRG neurons. The firing rates were modeled as linear functions of the foot position, velocity, and speed. We measured the accuracy of these encoding models by computing the coefficient of determination (R^2) between the actual and predicted firing rates using ten-fold cross validation. We examined the S1 neural response to replay stimulation patterns in two ways. First, we measured the similarity of neuronal responses on individual S1 channels across the movement and replay conditions by computing the product-moment correlation between the pairs of firing rate histograms, which we refer to as replay correlations. Second, we used multivariate linear regression to estimate foot speed from the entire population of neurons recorded in S1, similar to the decoding method used in [18], for both the movement and replay stimulation trials. Since the foot was not moving during the replay stimulation trials, the S1 neural responses were driven only by the sensory input provided by the replay stimulation.

We analyzed S1 neural responses from fabricated pattern trials using a Naïve Bayes Classifier [19] to determine how accurately we could detect a response (i.e. a difference from baseline) or discriminate responses evoked by pairs of different stimulus patterns. The

mean of the LFPs within a 100 ms window immediately following the stimulus onset were used as the features for Naïve Bayes classification with leave-one-out cross-validation.

B. S1 neuronal responses to active limb movement in awake monkeys

1) Experimental setup—We trained rhesus monkeys to perform a random target pursuit task using a two-link planar manipulandum while seated in a primate chair. A cursor displayed on the screen tracked the position of the manipulandum as it moved within a 20 cm square workspace. A series of 2 cm square targets appeared at any location within the workspace. A tone was delivered when the monkey moved the cursor into a target and the next target was displayed. Following eight successful target acquisitions, the monkey received a liquid reward. A depiction of the behavioral setup is shown in Figure 2A and a sample hand trajectory in 2B.

2) Surgical procedures—After a monkey could perform the behavioral task proficiently, we implanted a 96 channel microelectrode array with 1 mm long, iridium-oxide coated electrodes (Blackrock Microsystems) in the post-central gyrus. We determined the proximal arm representation in area 2 intra-operatively through examination of the gross anatomy, stimulating primary motor cortex to find proximal arm representation, and recording from the surface of the post-central gyrus to identify proprioceptive responses. In each surgery, the specific implant site was chosen to maximize the proximal arm representation while avoiding cerebral vasculature.

Once a specific implant site was chosen, the array was pneumatically inserted using methods that have been described elsewhere [20]. All surgery was performed under isoflurane gas anesthesia (1–2%) except during intra-operative stimulation and recording, during which the monkey was transitioned to remifentanil (0.4 μg/kg/min continuous infusion). The monkey was administered antibiotics, anti-inflamatories, and buprenorphine for several days after surgery and given at least 7 days to recover before beginning experiments.

3) Data collection—We recorded from the microelectrode array with a multi-channel data recording system (MAP, Plexon, Inc., Dallas, TX). Thresholded waveforms, position signal and timing of behavioral task events (rewards and target acquisitions) were recorded for offline analysis. The position of the handle was sampled at 1000 Hz with a spatial resolution of approximately 200 μm. Velocity and acceleration signals were obtained by digitally low pass filtering the position signal (8-pole Butterworth, 10 Hz corner) and differentiating. We discriminated single neurons using Plexon Offline Sorter (Plexon, Inc.).

4) Receptive field mapping—For two datasets, after recording was complete, the monkey was lightly sedated with ketamine (5 mg/kg). We classified the receptive fields (RFs) of individual neurons as either cutaneous or deep, based on their responses to mechanical stimulation of the monkey's arm. A cell was deemed to be cutaneous if it responded to displacement of hairs on the arm or torso or to light touch of the skin. A unit was considered to have a deep RF if it responded only to manipulation of the limb or deep palpation of the muscles. Neurons for which we could not find a clear RF were classified as unknown.

5) Single cell data analysis—In order to determine the lag at which a particular neuron optimally represented limb kinematics we used a generalized linear model (GLM) with a Poisson distribution and a log link function [21] shown in equations 1 and 2. The independent variable ($\mathbf{x}$) was a six-element vector representing kinematic state of the limb, including a 1 (to model the baseline firing rate), x and y position, x and y velocity, and speed. In Equation 2, $\mathbf{x}$ again represents kinematic state vector and β the set of weights that

best describe the particular neuron being fit. We then evaluated the likelihood of the observed spike train given our predicted firing rate for a range of lags between limb state and discharge rate (See: [21] for likelihood calculation). We defined the log-likelihood ratio as the ratio of the log likelihood given our model to the likelihood of a null-model that assumes a constant firing rate for the duration of the dataset.

$$P(s|\mathbf{x})=\frac{\lambda^s e^{-\lambda}}{s!} \quad (1)$$

$$\lambda=\exp(\mathbf{x}\cdot\beta) \quad (2)$$

6) Neural population data analysis—We decoded end-point kinematics from S1 discharge using a Wiener filter with 10, 50 ms bins distributed symmetrically about zero. We judged the goodness of fit for these decoded kinematics by computing the coefficient of determination (R^2) between the actual and predicted kinematic trajectories using ten-fold cross validation after removing periods of inactivity lasting longer than five seconds.

To evaluate the extent to which neurons with cutaneous and deep RFs contributed to our ability to decode kinematics we conducted a neuron dropping experiment. We removed individual neurons and retrained the decoder, repeating the process for each neuron. We considered the neuron that, when removed, resulted in the lowest R^2, to have been the most uniquely informative neuron. We then repeated the entire process, removing both this and a second neuron to find the second most uniquely informative neuron. This process was repeated until there were no neurons remaining.

7) ICMS detection task—We tested a monkey's ability to detect brief trains of stimuli delivered through electrodes implanted in area 2. Monkeys were initially trained to move the cursor to a central target and wait a random time (0.5 to 5 seconds) before receiving a force perturbation to the handle. It then has 1 second to move to a second target to receive a reward. Following training, ICMS(400 ms, 300 Hz train of symmetric, bipolar pulses, 200 μs/phase) was substituted for the mechanical perturbation.

III. Results

A. Neural responses in S1 to PAMS in feline DRG

We made recordings in S1 to measure neuronal responses evoked by PAMS in the DRG. The replay pattern stimuli were used to evaluate the S1 neuronal response to naturalistic patterns of stimulation. The fabricated pattern stimuli were used to examine the sensitivity of the S1 response to variations in the intensity, pulse-rate, and location of stimuli applied in the DRG.

1) Tuning Properties of DRG Neurons—The DRG neuronal recordings provided movement-related sensory input patterns for the replay stimulation trials. To verify that these patterns of sensory activity encoded information about limb-state, we modeled the firing rates of DRG neurons as a function of foot position, velocity, and speed, separately and in combination. Only the horizontal and vertical components of the foot kinematics were used as the motion was restricted to the parasagittal plane. Figure 3A shows an example of the actual firing rate response of a single DRG channel during a center-out movement. The dashed trace shows the firing rate predictions based on the combined model, and tested with 10-fold cross validation. The linear model captured the neural response quite

accurately ($R^2 = 0.61$), including the large peaks in firing rate that occurred during the transitory phases as well as variations in the steady-state firing rate corresponding to different hold positions during the center-out-and-back movements.

Figure 3B shows a summary of the R^2 values from the 142 DRG channels that we examined. In general, the combined model was much better than those based only on position, velocity, or speed, suggesting that most neurons encode multiple state variables. This is not surprising, considering that Ia muscle spindle afferents are known to encode both the length and rate of muscle stretch, thus simultaneously conveying joint position and velocity information [22].

2) S1 response to naturalistic patterns of PAMS—The spike-rate histogram at the top of figure 4A shows the firing rate of a unit in S1 during passive motion (green) and replay PAMS (red) conditions (cat 1). The kinematics for the foot are shown at the bottom of panel A. The firing rate of this unit was highly correlated with the foot speed ($R^2 = 0.59$), exhibiting a burst of activity during both the outward and inward directions of the movements. Replay PAMS was applied on 15 channels in the DRG. The pattern of stimulation pulses applied to each DRG channel is shown in the raster plot in Figure 4A. Each tick mark in this plot represents a stimulation pulse (7 μA pulses for each channel). During the replay trial, the unit exhibited a strong burst of activity during the 1st and 4th phases of the corresponding movement, but was silent during the other phases. The replay correlation, which measures the similarity of the firing rate histograms for the motion and replay conditions was $r = 0.31$.

Since several of the S1 neurons were highly correlated with foot speed during the passive motion trials, it was possible to build a neural decoder that estimated foot speed from S1 neural activity. Figure 4B shows that the decoder was highly accurate ($R^2 = 0.97$) in estimating foot speed (black trace) during the movement condition (green trace) and that the S1 neural activity recorded during the replay condition also enabled a good estimate of foot speed ($R^2 = 0.66$, red trace). It was also possible to decode foot position accurately (horizontal: $R^2 = 0.93$; vertical: $R^2 = 0.76$) and velocity (horizontal: $R^2 = 0.82$; vertical: $R^2 = 0.68$) from this S1 population during the replay trials.

Figure 4C illustrates the reliability of the S1 response across repeated applications of the same stimulus pattern (cat 4). The raster plot at the top shows the response recorded on a single S1 channel during 28 repetitions of a flexion-hold-extension motion; the average leg length and speed profiles are shown at the bottom. The second raster plot shows the response on the same S1 channel during 28 repeated applications of the replay pattern, which consisted of 30 DRG channels (14 electrodes in L6 and 16 in L7; 7 μA stimulation pulses on each channel). The firing rate histograms for the motion and replay trials are shown below the raster plots. During the motion trials, this unit exhibited a sustained burst of activity during both the flexion and extension phases of the motion trial. The unit responded similarly during the replay trials (replay correlation = 0.48), although the timing and duration of the responses differed a bit from the motion trials.

3) Sensitivity of S1 response to variations in PAMS intensity, pulse-rate, and location—In cats 2 and 3, we tested several simple patterns of PAMS to examine the sensitivity of the S1 neuronal response to variations in the intensity, pulse-rate, and location of stimuli applied in the DRG. S1 neural responses were used as inputs to a Naïve Bayes Classifier [19]. Figure 5A shows classification accuracies for stimulation patterns that varied in amplitude (5 levels between 3 and 20 μA) and location (5 different electrode pairs); the pulse-rate was fixed at 20 pps for panels A and B.

Four input locations (columns 1,2, 4, and 5 in figure 5A) evoked S1 responses that could be detected from the background discharge with high reliability (>90%), even at intensities as low as 3 μA. Accurate discrimination between the effects of two adjacent stimulus locations was also possible (panel B). Interestingly, panel B shows a non-monotonic relationship between classification accuracy and stimulation amplitude – intensities above 11.5 μA and below 7.2 μA had lower classification accuracies. Thus, while high-intensity stimulation may evoke stronger responses in S1, the ability to distinguish different input locations, particularly ones adjacent to each other as in (B), may degrade at higher stimulation intensities. This degradation may be due to the recruitment of larger and potentially nonhomogeneous populations of afferent neurons resulting in less discriminable patterns of activity in S1.

We also examined the effect of varying the stimulus pulse-rate. The matrix plot in figure 5C shows the classification accuracies for discriminating pairs of stimuli having different pulse-rates, with the amplitude fixed at 6 μA and stimulating on all 16 DRG channels. The top, left square in this matrix shows that the S1 responses to 200 pps could be distinguished with high accuracy from those evoked by 1000 pps stimuli with high accuracy. In general, stimulation frequency differences greater than 400 pps were clearly distinguishable even up to rates of 1000 pps. The inset in panel C shows an example of the multiunit response to stimulation at these frequencies. These results indicate that fabricated patterns of PAMS elicited responses in S1 that were broadly responsive and sensitive to variations in the stimulus pulse-rate, even those well beyond the normal physiological range for DRG neuron spike rates.

B. Area 2 representation of active limb movement

We analyzed a database consisting of 259 neurons in five datasets recorded from four monkeys designated A, M, P, and T. Two data sets (one from each hemisphere) were recorded from Monkey T and denoted T1 and T2. All neurons from each dataset were recorded simultaneously, and the recordings lasted between 10 and 60 minutes.

1) Tuning Properties of Individual Neurons—Figure 2B shows the discharge of two neurons recorded during the random target task. Each colored dot corresponds to an action potential that occurred along the hand path. This pictured path represents 6.5 seconds of data. Although there was a tendency for spikes to be clustered around movement directions within 45 degrees of a preferred direction, the stochastic nature of the discharge makes this difficult to appreciate in this short segment. GLM fits to 58 minutes of data for these two example neurons are shown in Figure 2C, including both the limb position- and movement-dependent components of the firing rate. In order to highlight the cosine tuning, the firing rate is plotted in polar, rather than Cartesian coordinates, with direction and speed along the bottom and vertical axes respectively. The model contains a speed term that makes the model different from a simple linear, cosine tuned model. Most notably, for cells with speed components greater than the norm of the velocity components, as was the case for 77 out of 259 cells (30%), the discharge rate increased with faster movements regardless of movement direction. Similar observations of speed tuning have been made of cells in motor cortex [23]. There were 42 cells (16%) for which the speed term was negative and greater in magnitude than the velocity component norm. These cells exhibited pause-like behavior, their discharge slowing for all movements, in a direction-dependent manner.

Although the properties of individual neurons can be determined by recording, there are currently no practical methods that allow individual neurons to be activated electrically. As a consequence, the perceptual effects of ICMS will necessarily be the result of the near-simultaneous activation of many cells and fibers surrounding the tip of the electrode. If these

neurons are highly heterogeneous with respect to their representation of limb state, it is unlikely that the monkey's perception will resemble that of natural limb movement. To address this concern, we have compared the PDs of pairs neurons recorded simultaneously from a single electrode to those of randomly selected pairs across electrodes. Figure 2D illustrates that neurons with PDs within 20 degrees were more than twice a likely on the same electrode compared to two different electrodes. The difference between the two distributions was highly significant ($p < 10^{-4}$; K-S test).

2) Timing of Informativeness—To evaluate the relative timing between the kinematics of active limb movement and activity in somatosensory cortex, we examined the log-likelihood ratio of the GLM fit over a range of lags between kinematics and neural discharge. In so doing, we generated plots of the log-likelihood ratio with respect to lag (Figure 6A). As expected, there was typically a peak near zero lag, in this case at −61 ms. The timing of this peak indicates the time at which the model was most predictive of firing rate. A peak to the right of zero (i.e., positive lag) implies that the neuron was most informative about movements of the limb in the recent past, as would be expected of a sensory cell. Those cells that had peaks with negative lag were predictive of future movements of the limb, like a motor cell.

Figure 6B shows a histogram of the time of the peak informativeness for all neurons. The distribution of these peaks spanned zero; that is, for some cells the timing of peak information was at positive lag while for others it was negative. This distribution indicates that some S1 neurons contain information similar to that provided by a cell in motor cortex, as has been shown previously [24]. This suggests that some proprioceptive neurons encode future active movements of the limb, perhaps reflecting efference copy inputs from the motor or premotor cortices.

3) Kinematic decoding—We were able to decode position and velocity of the limb endpoint from somatosensory neural activity using each of the datasets. Because many neurons carried information about upcoming limb movements, we used noncausal Wiener filters that spanned time zero. One such set of decoded kinematics is shown in Figure 7. The average accuracy of prediction in terms of R^2, was 0.59 and 0.66 for position (panel A) and velocity (panel B) respectively. Acceleration could also be decoded, but somewhat less accurately ($R^2 = 0.44$). The accuracy of decoded kinematics for all datasets and all variables is summarized in Figure 7C (mean ± standard deviation across folds).

4) Informativeness of neurons to kinematic decoding: no effect of RF type—To evaluate how much each neuron contributed to the decoded kinematics we performed a neuron dropping experiment. As shown in Figure 8, the decoding accuracy decreased steadily as neurons were dropped. This steady decline indicates that the ability to decode kinematics was not the result of a small number of highly informative neurons. If that were the case we would have seen a sudden drop off in accuracy after those few useful neurons were no longer included.

We also evaluated the role played by neurons with different receptive field types by noting whether the most informative neurons had a proprioceptive or cutaneous RF. The color of the error bars in figure 8 indicates which RF type was dropped at the previous step. The intermingling of RFs throughout the curve indicates that both types of neurons were important for accurate predictions. The drop order was not significantly biased (Wilcoxon rank-sum p=0.43 (array P) p = 0.60 (array T2)) by RF type. This suggests that both proprioceptive and cutaneous neurons carry useful information about limb kinematics.

5) Detection of stimulation within area 2—We have begun a preliminary series of psychophysical experiments testing the effects of ICMS in monkey P. The monkey had been trained simply to detect a brief torque pulse delivered to the handle of the manipulandum as it was held for a random period (0.5 to 5.0 seconds) within a central target. Following the pulse, the monkey had 1.4 seconds to move the handle into a second target window. Following training, a 400 ms ICMS train (300 Hz, 200 μs biphasic pulses) was delivered in place of the force pulse. Figure 9A shows the monkey's performance for a range of different currents applied to a single electrode. The monkey detected ICMS trains with currents above 30 μamps with essentially 100% reliability. Panel B shows data from a separate session several days later, in which any of six different electrodes were stimulated at 80 μamps. Detection rate for electrode #57 remained at 100%, the same rate achieved for two other electrodes. Detection rate for electrode #10 was not as reliable, while electrodes #67 and #89 were no more effective than chance.

IV. Discussion

A. The need for afferent feedback in BMI applications

Significant progress has been made over the last two decades to advance the mechatronics of prosthetic limbs, including the use of both myoelectric [25] and brain control [3, 7, 26–31]. However, most of these interfaces fail to provide any somatosensory feedback to the user (see [32] for an important exception). Historically, this lack of feedback has caused users of upper limb prostheses to prefer less technologically advanced, body-powered limbs because of the sense of effort, or "extended physiological proprioception" provided by the cable drive systems [33, 34]. In the absence of such feedback, even the most advanced prosthetic device is likely to remain a numb, extracorporeal tool, rather than a fully integrated functional limb.

Although the senses of touch and proprioception are considered together as twin components of the somatosensory system, they present rather different objectives and challenges. We are keenly aware of the sense of touch. We use it to detect contact, distinguish textures, and identify grasped objects. It also acts at a more subconscious level to prevent a grasped object from slipping. Proprioception, on the other hand, works primarily at a subconscious level. We are only dimly aware of this modality, yet it is critical for both movement planning and execution [35, 36]. Proprioception includes information about end point and muscle forces as well as the configuration of the limb [37–41]. Despite their evident differences, the information conveyed by these two modalities overlaps in unexpected ways, as in the prediction of kinematic limb state from neurons having both cutaneous and proprioceptive receptive fields ([42]Figure 8). Spinal reflexes depend on input from both types of receptors, and the cerebellum as well as the cerebral cortex processes inputs from both receptor types. Understanding the details of this distributed processing will be critical to the design of a prosthesis that can provide both the conscious and subconscious aspects of somatosensation.

B. Strategies for developing a somatosensory interface

The goal of this paper was to highlight some of the challenges facing development of a somatosensory afferent interface and to present initial results from two complementary approaches based on microstimulation of neuronal populations in either the DRG or S1. Since the function of the afferent interface is to transmit limb-state information to the central nervous system (CNS), it is necessary to devise strategies for encoding this information in spatiotemporal patterns of stimulation. As a first step, we examined the association between neural firing rate (in S1 and DRG neurons) and limb-state variables, including position, velocity, and acceleration. More advanced encoding and decoding models that account for

nonlinearities in these relationships might be expected to perform better, although this has not consistently been true of kinematic decoder models based on M1 discharge [43–45]. However, the purpose of this analysis was to examine simple (i.e. linear) associations between the limb state variables and the corresponding neural firing rates and to identify those state variables most strongly correlated with neural firing. This information can provide the initial basis for patterning electrical stimulation intended to encode limb state. As these experiments progress, it may become necessary to develop better encoding models, but at this early stage we are assuming that the spatiotemporal stimulation pattern will provide only a crude approximation of the actual encoding processes at best. A relevant comparison can be made to the development of cochlear implants. Much of the contemporary work in cochlear implant technologies focuses on improving the algorithms that encode various features of the acoustic signal [42], yet the earliest studies used encoding models that simply mapped pitch perceptions to stimulation on specific electrodes [46].

An important challenge is in evaluating the effects of stimulation in delivering ‘meaningful’ signals to the CNS. Unlike work with human subjects who can describe the sensation(s) evoked by stimulation, work with animals presents a unique experimental challenge. We are taking two different approaches to this problem in our work with DRG stimulation in anesthetized cats and cortical stimulation in awake monkeys. Lacking the ability to interrogate the animal about the similarity of limb movement and PAMS, we can nonetheless use the cortical response to each as a measure of their similarity. Multichannel neural recordings in S1 provide a convenient method for quantifying the nature of the signals transmitted to the brain from the periphery. We do have the means to interrogate the awake monkey about the effect of stimulation, but only indirectly. Psychophysical experiments have revealed that the frequency of stimulation within area 3b, a region of S1 that processes tactile signals, can be used to evoke apparently realistic tactile perceptions of flutter vibration in monkey subjects. These monkeys were able to compare the frequency of electrical stimulation with that of mechanical vibration [47]. The ICMS results reported here were focused exclusively on measuring the detectability of stimuli applied to different electrodes. In our current work, we are beginning to address the interaction of stimulus effects through different electrodes and the nature of the evoked percept.

C. The use of peripheral stimulation to evoke meaningful somatosensory stimulation

Direct evidence supporting the feasibility of peripheral nerve microstimulation as a viable afferent interface for neuroprostheses has been provided by the studies of Dhillon and Horch[12, 48]. They were able to evoke discriminable sensations of touch, joint movement, and position by stimulating through longitudinal intrafascicular (LIFE) electrodes that had been implanted semi-chronically in the peripheral nerve stump of long-term amputees. Likewise, microstimulation during acute microneurography is reported to evoke precisely localized sensations of flutter-vibration and pressure in humans [9–11].

That PAMS is a peripheral stimulation technique may be one of its principle advantages. This technique activates neurons at the lowest level of the sensory neuraxis. In doing so, higher levels of the sensory neuraxis that receive (direct or indirect) inputs from these primary afferents can participate in the processing of the information encoded in the pattern of PAMS. For example, stimulating primary afferent fibers provides short latency access to the cerebellum via the spinocerebellar tracts, a consideration that may be particularly important for the control of movement independently of the user’s conscious awareness.

One of the key findings of the PAMS experiments described above is that stimulation of the DRG can evoke patterns of activity in S1 that, despite their complexity, are fairly well correlated with those generated during passive movement (Figure 4A). Although the magnitude of correlation was modest, we feel these results are encouraging considering that

we used only 15 channels of stimulation. In those experiments, the stimulation intensity was 7 μA on each channel, which is approximately twice the threshold for activating a single primary afferent fiber in the DRG with this technique [14]. While we cannot determine the exact number of primary afferent fibers that were activated by each electrode, we can assume that these represent only a small fraction of the total population of primary afferents that would be active during normal motion of the leg. Stimulation of more electrodes at lower intensity might well improve control.

The limitations of the 'replayed' input are evident when examining the single-unit responses in S1 (Figure 4A), which show periods of inactivity not present in the movement condition. This suggests that important portions of the afferent input were missing or too weak to evoke a response from the S1 neuron. Our current experiments are aimed at developing strategies to strengthen the effects of stimulation while preserving the natural spatiotemporal patterns of afferent activity. Increasing the stimulation intensity will recruit a larger number of fibers, but likely at the cost of further decreased precision. Indeed, our experiments using 'fabricated' patterns of stimulation demonstrate the importance of using low-intensity stimulation to preserve the spatial features of the inputs (see Figure 5B). Another strategy is to amplify the stimulation pulse rate, preserving the temporal profile of activity but strengthening the total synaptic input received by downstream neurons. Better methods of quantifying the cortical effects of stimulation may be necessary to identify the most effective method for patterning stimulation. For example, information theoretic measures such as mutual information may be advantageous as these can be used without assuming a specific form for the encoding model, as has been shown for M1 neurons [49]. Furthermore, spike-train similarity metrics such as those described in [50] may be more useful than simple linear correlations.

Our studies with fabricated patterns of stimulation also show that the neuronal discharge in S1 can be modulated by stimulation pulse-rates ranging from 20 to 1000 pps (Figure 5C). This is consistent with the studies cited above, in which human subjects reported graded sensations with stimulus rates as high as 1000 pps[13]. Although such high rates are well beyond the normal physiological range of firing rates, they may actually be perceived as more nearly natural due to the more stochastic pattern of neural firing generated by high-frequency stimulation as compared to lower frequencies, which recruit neural activity that is tightly phase-locked to the stimulation [51]. However, further studies in awake, behaving animals are needed to determine the nature of the perceptions, and the quality of the motor control generated by these different patterns.

D. Limb state representation within S1 and its application to ICMS for afferent feedback

Despite its potential advantages, DRG stimulation is of no use to a patient with a spinal cord injury, which requires access to a more central location such as the cerebral cortex. Our primate recordings were restricted to area 2, a region within S1 that receives input from area 3a as well as from the thalamus. As such, it likely represents a higher level of processing than does 3a. It is possible that accessing the nervous system at this level would activate a higher level, multi-modal percept, and circumvent the need to activate many highly distributed, labeled line inputs within the DRG.

The information encoded by area 2 neurons was well correlated with the kinematics of the monkey's limb, most strongly so with hand velocity, and to a lesser extent, position. Similar, less quantitative observations have been made before [41, 52]. We were able to make accurate predictions of limb state using relatively few neurons (Figures 7–8). Importantly, these predictions depended as much on neurons with classically defined cutaneous receptive fields as they did on proprioceptive neurons. Conversely, we were able to predict the discharge of single neurons based on a relatively simple model of kinematic limb-state

(Figure 2). These combined results suggest a convergence of submodalities that might simplify the problem of encoding a high level representation of limb state through stimulation in area 2. We have some preliminary evidence (not shown here) that a given cell's strongest response to perturbation of the hand is approximately aligned with its preferred direction for active movements. These results are in accord with those described earlier [41]. This alignment may further simplify any stimulus encoding scheme.

Unlike neural recording however, which allows information to be extracted from single cells, there currently exist no methods to achieve large scale activation of single cells in cortex. As a consequence, when using ICMS, perhaps even more so than with PAMS, we must rely on the homogeneity of the response properties of the cluster of cells activated by the stimulation. Primary visual cortex is organized into functional columns, each with a restricted receptive field and typically processing a particular submodality[53, 54]. This columnar organization was actually first described in area 3b, a tactile region of S1 [55]. Our evidence that PDs recorded from a single electrode tend to be aligned (Fig. 2D) is consistent with these observations, and lends encouragement to the goal of evoking natural physiological perceptions by stimulation in area 2. However, there is recent evidence suggesting that electrical stimulation activates neurons more sparsely and at a greater distance from the electrode tip than previously thought [56]. This property would further complicate the use of ICMS. As with PAMS, we anticipate that we will be able to optimize the ICMS effects through the use of large numbers of electrodes, each stimulated at relatively low current.

Optogenetics offers an exciting new method that may be superior to electrical stimulation for providing selective activation of neurons in the CNS [57]. With optogenetic methods, it is possible to target specific cell types, or cells with particular targets, for infection with viral vectors that incorporate light-sensitive ion channels (e.g., channel rhodopsins) into the cell membrane. Optical stimulation of these modified cells can cause rapid depolarization or hyperpolarization, depending on the specific channel rhodopsin used [58, 59]. Thus, it is possible to excite or inhibit specific types of neurons using different wavelengths of light, providing highly precise control over the pattern of neural activation for encoding information by an afferent interface.

Even without the ability to activate single neurons or classes of neurons, we and others have shown that it is possible to train monkeys to detect stimulation in areas 3a[60], 3b and 1 [61] 1, and now area 2. Monkeys have also been trained to distinguish stimuli of different frequencies within area 3a [60] and 3b, and different spatiotemporal patterns in 3b [61]. There is no indication from these experiments, however, that the stimulation elicited something resembling a normal sensation. However in another series of experiments, Romo and his colleagues used electrical stimulation within a column of quickly adapting neurons in area 3b to mimic the natural sense of mechanical vibration applied to the fingertip [62]. In those experiments, psychometric curves measuring the sensitivity to frequency differences had essentially the same shape for electrical and mechanical stimuli.

It might well be argued that vibration sense is a special case, well suited to the phase locking that electrical stimulation would induce. However, stimulation in the higher order visual areas MT and MST provides further evidence that ICMS may be used to mimic a natural sensation. In those experiments, monkeys were trained to distinguish the mean direction of motion of a partially coherent random dot display [63–65]. On some trials, a 200 Hz, 10 μA ICMS train was applied, which biased the monkey's perception of motion in the preferred direction of the stimulated neurons. Interestingly, currents of 80 μA often proved less effective, probably because they activated a larger, non-homogeneous group of cells [66]. We intend to pursue analogous experiments using ICMS in areas 3a and 2.

V. Conclusion

Somatosensory feedback is crucial for achieving stable and adaptive motor control, particularly for grasp and manipulation tasks where visual feedback alone is insufficient. Lacking proprioceptive feedback, patients with large-fiber sensory neuropathies exhibit severe impairments in the coordination of movements at multiple joints [35] and a degradation in the accuracy of movements performed without visual guidance [67]. Loss of tactile sensation is associated with other problems as well, such as chronic pain and damage to hands and feet. Creating a neural interface that restores at least some useful level of tactile and proprioceptive feedback will be a major challenge. A first step toward replacing this lost sense is to develop reliable mappings from limb state to cortical activity. These maps could be used to encode stimulus trains delivered via PAMS or ICMS, much like the analogous efferent maps are used to decode motor intention. Results presented here and from previous studies in animals [60–62, 68, 69] and humans [12, 70, 71] support the feasibility that such approaches can be used to provide meaningful sensation for conscious perception and control of movement. However, no experimental approach as yet, has addressed the question of whether the stimulation evokes proprioceptive-like sensations, or whether the input can be used to guide movement. These questions are intended for further future work with behaving animals.

Acknowledgments

This work was supported in part by the NIH grants 1R01-EB007749 and 1R21-NS-056136 and TATRC grant W81XWH-07-1-0716 to DJW. Funding for LEM provided by NIH grant 1R01-NS048845.

References

1. Farrell TR, Weir RF, Heckathorne CW, Childress DS. The effects of static friction and backlash on extended physiological proprioception control of a powered prosthesis. J Rehabil Res Dev. May-Jun;2005 42:327–41. [PubMed: 16187245]
2. Sainburg RL, Ghilardi MF, Poizner H, Ghez C. Control of limb dynamics in normal subjects and patients without proprioception. J Neurophysiol. 1995; 73:820–35. [PubMed: 7760137]
3. Serruya MD, Hatsopoulos NG, Paninski L, Fellows MR, Donoghue JP. Instant neural control of a movement signal. Nature. Mar 14.2002 416:141–2. [PubMed: 11894084]
4. Chapin JK, Moxon KA, Markowitz RS, Nicolelis MA. Real-time control of a robot arm using simultaneously recorded neurons in the motor cortex. Nat Neurosci. Jul.1999 2:664–70. [PubMed: 10404201]
5. Carmena JM, Lebedev MA, Crist RE, O'Doherty JE, Santucci DM, Dimitrov D, Patil PG, Henriquez CS, Nicolelis MA. Learning to Control a Brain-Machine Interface for Reaching and Grasping by Primates. PLoS Biol. Nov.2003 1:193–208.
6. Hochberg L, Serruya M, Friehs G, Mukand J, Saleh M, Caplan A, Branner A, Chen D, Penn R, Donoghue J. Neuronal ensemble control of prosthetic devices by a human with tetraplegia. news@nature. Jul 13.2006 442:164–71.
7. Pohlmeyer EA, Oby ER, Perreault EJ, Solla SA, Kilgore KL, Kirsch RF, Miller LE. Toward the restoration of hand use to a paralyzed monkey: brain-controlled functional electrical stimulation of forearm muscles. PLoS One. 2009; 4:e5924. [PubMed: 19526055]
8. Santhanam G, Ryu SI, Yu BM, Afshar A, Shenoy KV. A high-performance brain-computer interface. Nature. Jul 13.2006 442:195–8. [PubMed: 16838020]
9. Torebjork HE, Schady W, Ochoa J. Sensory correlates of somatic afferent fibre activation. Hum Neurobiol. 1984; 3:15–20. [PubMed: 6330006]
10. Ochoa J, Torebjork E. Sensations evoked by intraneural microstimulation of single mechanoreceptor units innervating the human hand. J Physiol. Sep.1983 342:633–54. [PubMed: 6631752]

11. Macefield G, Gandevia SC, Burke D. Perceptual responses to microstimulation of single afferents innervating joints, muscles and skin of the human hand. J Physiol. Oct.1990 429:113–29. [PubMed: 2148951]
12. Dhillon GS, Horch KW. Direct neural sensory feedback and control of a prosthetic arm. IEEE Trans Neural Syst Rehabil Eng. Dec.2005 13:468–72. [PubMed: 16425828]
13. Dhillon GS, Kruger TB, Sandhu JS, Horch KW. Effects of short-term training on sensory and motor function in severed nerves of long-term human amputees. J Neurophysiol. May.2005 93:2625–33. [PubMed: 15846000]
14. Gaunt RA, Hokanson JA, Weber DJ. Microstimulation of primary afferent neurons in the L7 dorsal root ganglia using multielectrode arrays in anesthetized cats: thresholds and recruitment properties. J Neural Eng. Oct.2009 6:12.
15. Schmidt E, Bak M, Hambrecht F, Kufta C, O'Rourke D, Vallabhanath P. Feasibility of a visual prosthesis for the blind based on intracortical microsimulation of the visual cortex. Brain. 1996; 119:507–522. [PubMed: 8800945]
16. Troyk P, Bak M, Berg J, Bradley D, Cogan S, Erickson R, Kufta C, McCreery D, Schmidt E, Towle V. A model for intracortical visual prosthesis research. Artif Organs. Nov.2003 27:1005–15. [PubMed: 14616519]
17. Landgren S, Silfvenius H. Projection to cerebral cortex of group I muscle afferents from the cat's hind limb. J Physiol. Feb.1969 200:353–72. [PubMed: 5764405]
18. Weber DJ, Stein RB, Everaert DG, Prochazka A. Limb-state feedback from ensembles of simultaneously recorded dorsal root ganglion neurons. J Neural Eng. Sep.2007 4:S168–80. [PubMed: 17873416]
19. Mitchell TM, Hutchinson R, Niculescu RS, Pereira X, Wang M, Newman S. Learning to Decode Cognitive States from Brain Images. Machine Learning. 2004; 57:145–175.
20. Pohlmeyer EA, Solla SA, Perreault EJ, Miller LE. Prediction of upper limb muscle activity from motor cortical discharge during reaching. J Neural Eng. Dec.2007 4:369–79. [PubMed: 18057504]
21. Pillow JW, Paninski L, Uzzell VJ, Simoncelli EP, Chichilnisky EJ. Prediction and decoding of retinal ganglion cell responses with a probabilistic spiking model. J Neurosci. Nov 23.2005 25:11003–13. [PubMed: 16306413]
22. Wagenaar JB, Ventura V, Weber DJ. State-space decoding of primary afferent neuron firing rates. J Neural Eng. Jan 19.2011 8:016002. [PubMed: 21245525]
23. Moran DW, Schwartz AB. Motor cortical representation of speed and direction during reaching. J Neurophysiol. 1999; 82:2676–92. [PubMed: 10561437]
24. Soso MJ, Fetz EE. Responses of identified cells in postcentral cortex of awake monkeys during comparable active and passive joint movements. J Neurophysiol. Apr.1980 43:1090–110. [PubMed: 6766995]
25. Kuiken TA, Li G, Lock BA, Lipschutz RD, Miller LA, Stubblefield KA, Englehart KB. Targeted muscle reinnervation for real-time myoelectric control of multifunction artificial arms. JAMA. Feb 11.2009 301:619–28. [PubMed: 19211469]
26. Velliste M, Perel S, Spalding MC, Whitford AS, Schwartz AB. Cortical control of a prosthetic arm for self-feeding. Nature. Jun 19.2008 453:1098–101. [PubMed: 18509337]
27. Wessberg J, Stambaugh CR, Kralik JD, Beck PD, Laubach M, Chapin JK, Kim J, Biggs SJ, Srinivasan MA, Nicolelis MA. Real-time prediction of hand trajectory by ensembles of cortical neurons in primates. Nature. Nov 16.2000 408:361–5. [PubMed: 11099043]
28. Schwartz AB. Cortical neural prosthetics. Annu Rev Neurosci. 2004; 27:487–507. [PubMed: 15217341]
29. Taylor D. Direct Cortical Control of 3D Neuroprosthetic Devices. Science. Jun 7.2002 296:1829–1832. [PubMed: 12052948]
30. Wolpaw JR, McFarland DJ, Neat GW, Forneris CA. An EEG-based brain-computer interface for cursor control. Electroencephalogr Clin Neurophysiol. Mar.1991 78:252–9. [PubMed: 1707798]
31. Leuthardt EC, Schalk G, Wolpaw JR, Ojemann JG, Moran DW. A brain-computer interface using electrocorticographic signals in humans. J Neural Eng. Jun.2004 1:63–71. [PubMed: 15876624]
32. Marasco PD, Schultz AE, Kuiken TA. Sensory capacity of reinnervated skin after redirection of amputated upper limb nerves to the chest. Brain. Apr 15.2009

33. Shannon G. A myoelectrically-controlled prosthesis with sensory feedback. Med Biol Eng Comput. 1979; 17:73–80. [PubMed: 312386]
34. Doubler JA, Childress DS. An analysis of extended physiological proprioception as a prosthesis-control technique. J Rehabil Res Dev. 1984; 21:5–18. [PubMed: 6527290]
35. Sainburg RL, Poizner H, Ghez C. Loss of proprioception produces deficits in interjoint coordination. J Neurophysiol. 1993; 70:2136–47. [PubMed: 8294975]
36. Sarlegna FR, Sainburg RL. The roles of vision and proprioception in the planning of reaching movements. Adv Exp Med Biol. 2009; 629:317–35. [PubMed: 19227507]
37. Tanji J. Activity of neurons in cortical area 3a during maintenance of steady postures by the monkey. Brain Res. May 9.1975 88:549–53. [PubMed: 124617]
38. Fromm C, Evarts EV. Pyramidal tract neurons in somatosensory cortex: central and peripheral inputs during voluntary movement. Brain Res. 1982; 238:186–91. [PubMed: 6805854]
39. Wolpaw JR. Correlations between task-related activity and responses to perturbation in primate sensorimotor cortex. J Neurophysiol. Dec.1980 44:1122–38. [PubMed: 6450275]
40. Yumiya H, Kubota K, Asanuma H. Activities of neurons in area 3a of the cerebral cortex during voluntary movements in the monkey. Brain Res. 1974; 78:169–77. [PubMed: 4211778]
41. Prud'homme MJL, Kalaska JF. Proprioceptive activity in primate primary somatosensory cortex during active arm reaching movements. J Neurophysiol. 1994; 72:2280–2301. [PubMed: 7884459]
42. McDermott HJ. Music perception with cochlear implants: a review. Trends in amplification. 2004; 8:49–82. [PubMed: 15497033]
43. Lawhern V, Wu W, Hatsopoulos N, Paninski L. Population decoding of motor cortical activity using a generalized linear model with hidden states. Journal of neuroscience methods. Jun 15.2010 189:267–80. [PubMed: 20359500]
44. Santhanam G, Yu BM, Gilja V, Ryu SI, Afshar A, Sahani M, Shenoy KV. Factor-analysis methods for higher-performance neural prostheses. Journal of neurophysiology. Aug.2009 102:1315–30. [PubMed: 19297518]
45. Kim SP, Sanchez JC, Rao YN, Erdogmus D, Carmena JM, Lebedev MA, Nicolelis MA, Principe JC. A comparison of optimal MIMO linear and nonlinear models for brain-machine interfaces. Journal of neural engineering. Jun.2006 3:145–61. [PubMed: 16705271]
46. Simmons FB. Electrical stimulation of the auditory nerve in man. Archives of otolaryngology. Jul. 1966 84:2–54. [PubMed: 5936537]
47. Romo R, Hernandez A, Zainos A, Brody CD, Lemus L. Sensing without touching: psychophysical performance based on cortical microstimulation. Neuron. Apr.2000 26:273–8. [PubMed: 10798410]
48. Dhillon GS, Lawrence SM, Hutchinson DT, Horch KW. Residual function in peripheral nerve stumps of amputees: implications for neural control of artificial limbs. J Hand Surg [Am]. Jul.2004 29:605–15. discussion 616-8.
49. Paninski L, Fellows MR, Hatsopoulos NG, Donoghue JP. Spatiotemporal tuning of motor cortical neurons for hand position and velocity. J Neurophysiol. Jan.2004 91:515–32. [PubMed: 13679402]
50. Victor JD. Spike train metrics. Current opinion in neurobiology. Oct.2005 15:585–92. [PubMed: 16140522]
51. Rubinstein JT, Wilson BS, Finley CC, Abbas PJ. Pseudospontaneous activity: stochastic independence of auditory nerve fibers with electrical stimulation. Hear Res. Jan.1999 127:108–18. [PubMed: 9925022]
52. Gardner EP, Costanzo RM. Properties of kinesthetic neurons in somatosensory cortex of awake monkeys. Brain Res. Jun 15.1981 214:301–19. [PubMed: 7237173]
53. Ts'o D, Frostig R, Lieke E, Grinvald A. Functional organization of primate visual cortex revealed by high resolution optical imaging. Science. Jul 27.1990 249:417–420. [PubMed: 2165630]
54. Livingstone MS, Hubel DH. Anatomy and physiology of a color system in the primate visual cortex. Journal of Neuroscience. 1984; 4:309. [PubMed: 6198495]

55. Powell TP, Mountcastle VB. Some aspects of the functional organization of the cortex of the postcentral gyrus of the monkey: a correlation of findings obtained in a single unit analysis with cytoarchitecture. Bull Johns Hopkins Hosp. Sep.1959 105:133–62. [PubMed: 14434571]
56. Histed MH, Bonin V, Reid RC. Direct activation of sparse, distributed populations of cortical neurons by electrical microstimulation. Neuron. Aug 27.2009 63:508–22. [PubMed: 19709632]
57. Gilja V, Chestek C, Diester I, Henderson J, Deisseroth K, Shenoy K. Challenges and Opportunities for Next-Generation Intra-Cortically Based Neural Prostheses. IEEE Trans Biomed Eng. Jan 20.2011
58. Boyden ES, Zhang F, Bamberg E, Nagel G, Deisseroth K. Millisecond-timescale, genetically targeted optical control of neural activity. Nat Neurosci. Sep.2005 8:1263–8. [PubMed: 16116447]
59. Zhang F, Aravanis AM, Adamantidis A, de Lecea L, Deisseroth K. Circuit-breakers: optical technologies for probing neural signals and systems. Nat Rev Neurosci. Aug.2007 8:577–81. [PubMed: 17643087]
60. London BM, Jordan LR, Jackson CR, Miller LE. Electrical stimulation of the proprioceptive cortex (area 3a) used to instruct a behaving monkey. IEEE Trans Neural Syst Rehabil Eng. Feb.2008 16:32–6. [PubMed: 18303803]
61. Fitzsimmons NA, Drake W, Hanson TL, Lebedev MA, Nicolelis MA. Primate reaching cued by multichannel spatiotemporal cortical microstimulation. J Neurosci. May 23.2007 27:5593–602. [PubMed: 17522304]
62. Romo R, Hernandez A, Zainos A, Salinas E. Somatosensory discrimination based on cortical microstimulation. Nature. 1998; 392:387–90. [PubMed: 9537321]
63. Celebrini S, Newsome W. Microstimulation of extrastriate area MST influences preformance on a direction discrimination task. J Neurophysiology. 1995; 73:437–448.
64. Salzman CD, Britten KH, Newsome WT. Cortical microstimulation influences perceptual judgements of motion direction. Nature. Jul 12.1990 346:174–7. [PubMed: 2366872]
65. Bisley J, Zaksas D, Pasternak T. Microstimulation of cortical area mt affects performance on a visual working memory task. J Physiology. 2000:187–196.
66. Murasugi C, Salzman C, Newsome W. Microstimulation in visual area mt: Effetcts of varying pulse amplitude and frequency. J Neuroscience. 1993; 13:1719–1729.
67. Sanes JN, Mauritz KH, Evarts EV, Dalakas MC, Chu A. Motor deficits in patients with large-fiber sensory neuropathy. Proc Natl Acad Sci U S A. 1984; 81:979–82. [PubMed: 6322181]
68. Hokanson, JA.; Wagenaar, JB.; Weber, DJ. Neuronal responses in somatosensory cortex to multichannel microstimulation of primary afferent neurons. Society for Neuroscience Annual Meeting; San Diego, CA. 2007. p. 728.10
69. Venkatraman, S.; Carmena, JM. Encoding the location of virtual objects using cortical microstimulation. Society for Neuroscience Annual Meeting; Chicago, IL. 2009. p. 181.16
70. Riso RR, Ignagni AR, Keith MW. Cognitive feedback for use with FES upper extremity neuroprostheses. IEEE Trans Biomed Eng. Jan.1991 38:29–38. [PubMed: 2026429]
71. Kuiken TA, Marasco PD, Lock BA, Harden RN, Dewald JP. Redirection of cutaneous sensation from the hand to the chest skin of human amputees with targeted reinnervation. Proc Natl Acad Sci U S A. Dec 11.2007 104:20061–6. [PubMed: 18048339]

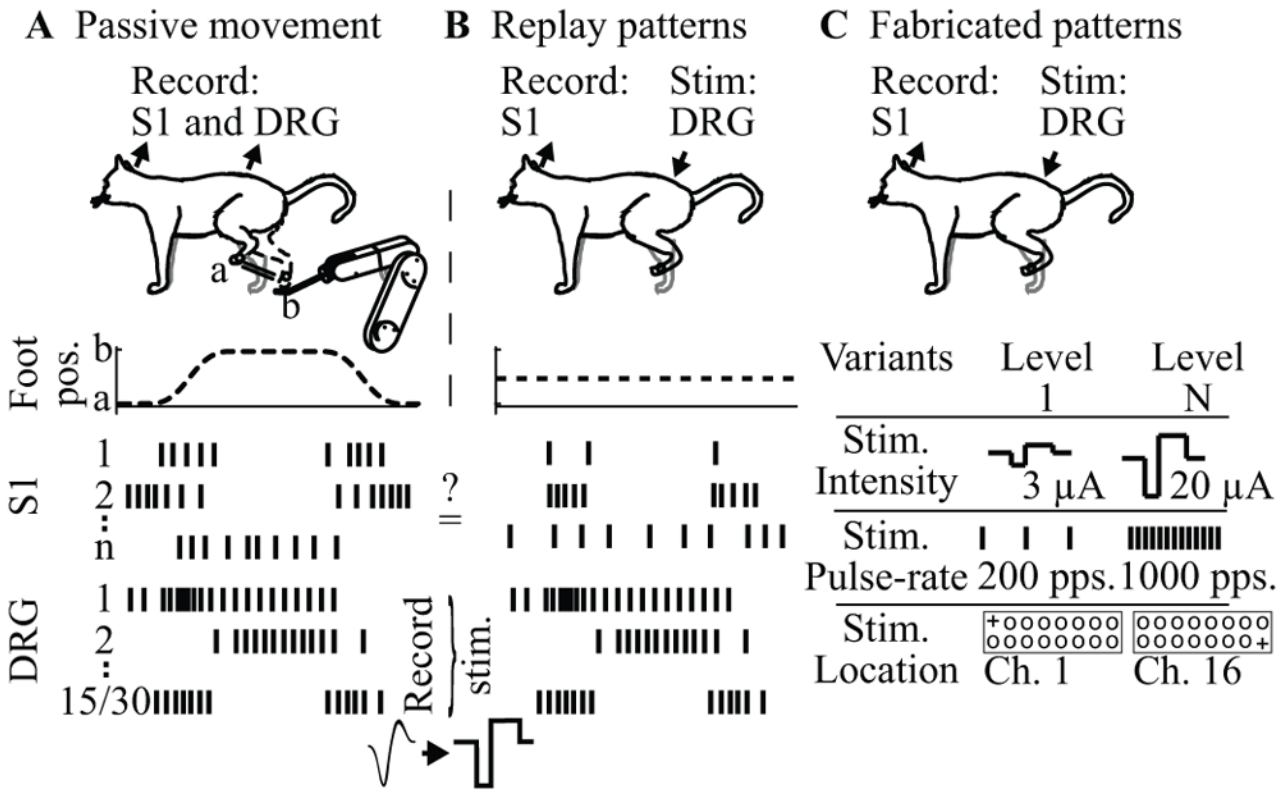

Fig. 1.

Setup for PAMS experiments in cats. (A) Replay pattern experiments begin with passive movement trials. (B) The pattern of DRG neural activity from the movement trials is used to generate a pattern of stimulation pulses applied to the same 15 (cat 1) or 30 (cat 4) DRG electrodes during the replay PAMS trials performed with the foot position fixed. (C). Simple patterns of PAMS are fabricated by systematically varying the intensity, pulse-rate, and location of active (+) electrodes (cats 2 and 3).

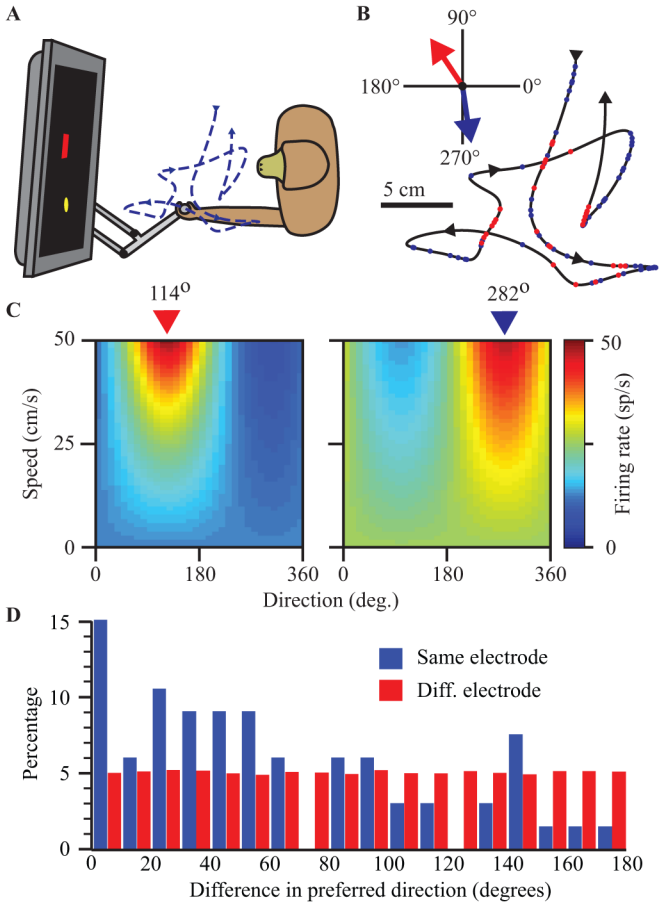

Fig. 2.

(A) Experimental setup for monkey experiments. (B) Hand trajectory during sequential random target task. Red and blue dots indicate firing of two neurons with PDs as indicated by colored arrows. Panels in (C) show the full tuning curves for two example neurons shown in (B) with PDs highlighted. (D) Differences in neuron preferred direction measured for pairs recorded from a single (blue) or across multiple (red) electrodes.

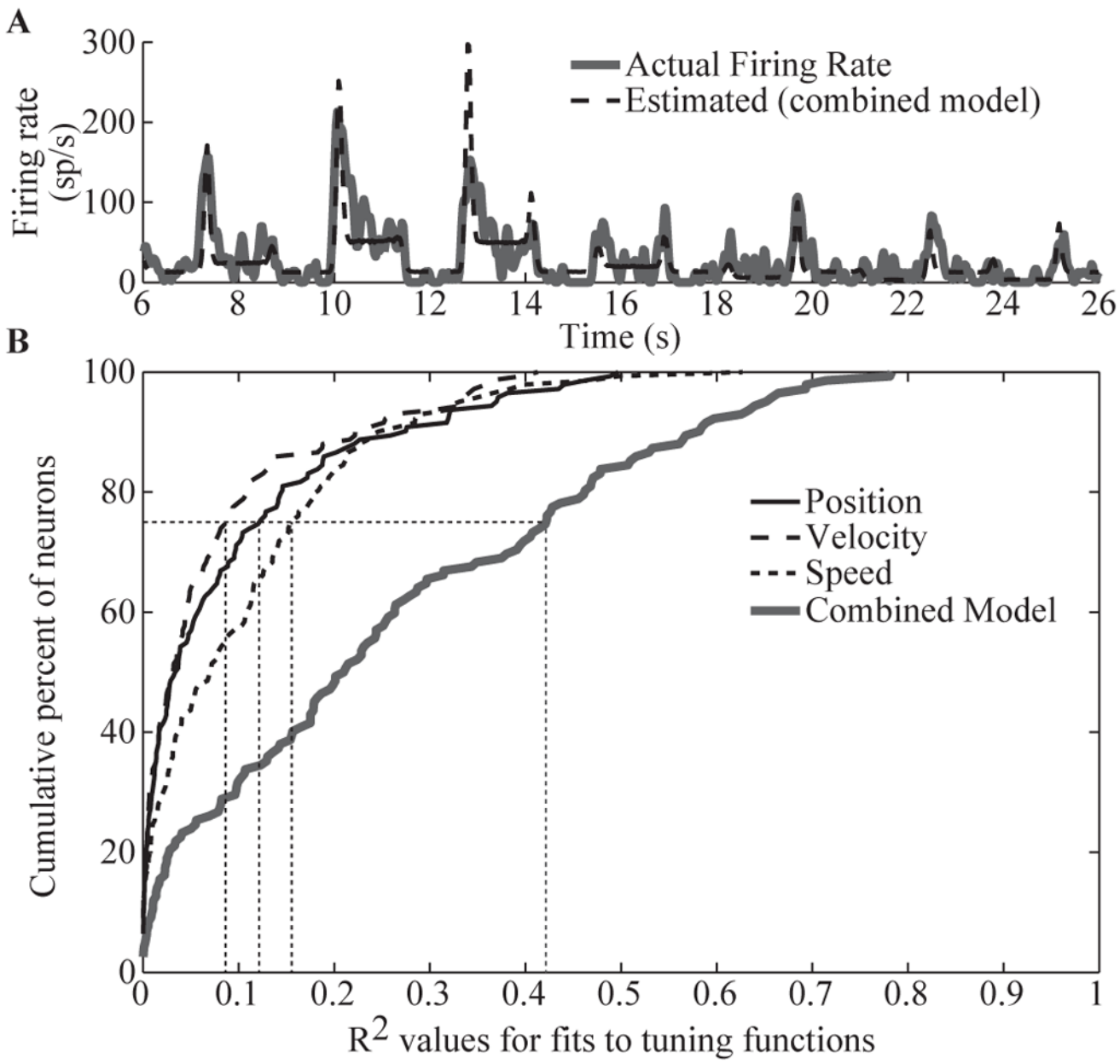

Fig. 3.

Limb-state encoding properties of DRG neurons during a center-out movement of the cat's foot. (A) Example of DRG neuron firing rate modeled as a linear function of foot position, velocity, and speed (i.e. combined model, $R^2 = 0.61$). (B) Cumulative distribution of R^2 values for tuning functions that include position, velocity, speed, or their combination (n = 142 neurons, cats 1, 2, and 3). The dotted vertical lines denote the 75th percentile for each model.

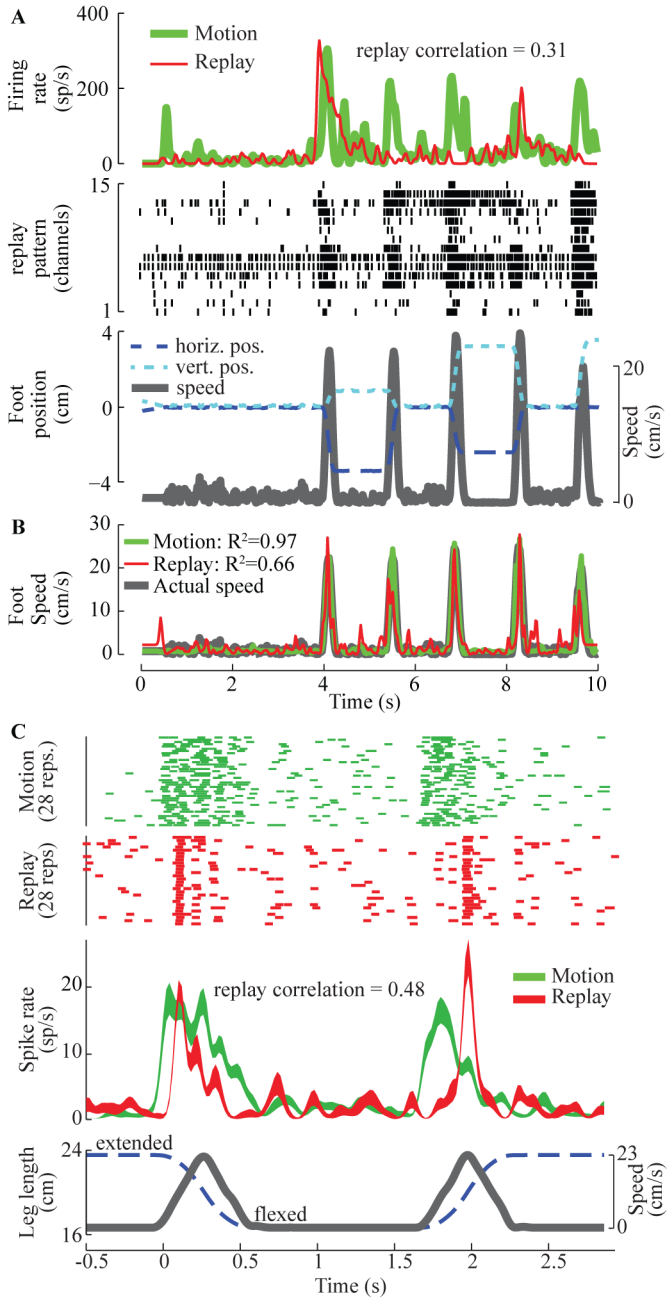

Fig. 4.

Results from PAMS replay pattern trials in cats. (A) Example of single-unit activity in S1 during passive movement and replay PAMS. Stimulation was applied on 15 channels in the L7 DRG (cat 1) following the pattern shown in the raster plot. Each tick in the replay pattern plot denotes a 7 μA pulse applied to 1 of the 15 channels in the L7 DRG. The position and speed of the foot during the movement trials are shown at the bottom of panel A. (B) Accurate decoding of foot-speed from S1 activity is possible in both the movement and replay conditions. (C) Consistency of the S1 response across 28 repetitions of the motion and replay PAMS stimulation patterns (cat 4). During the motion trials, the leg was moved passively between near full extension and flexion.

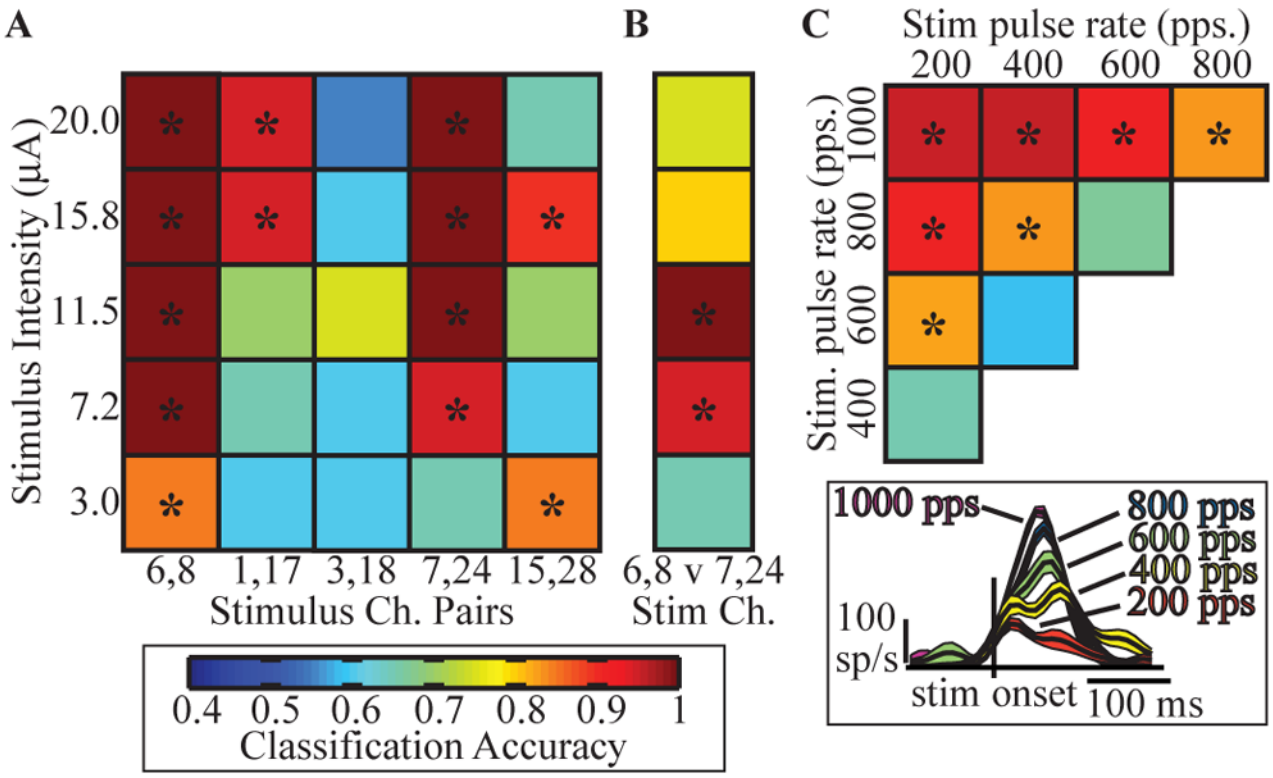

Fig. 5.

Discriminability of S1 neuronal responses to fabricated patterns of PAMS in cats. (A) S1 LFP response detection accuracy for PAMS of 5 different amplitudes (rows), applied to different DRG electrode locations represented by pairs of active electrodes (columns) and (B) classification accuracy of the effects of two stimulation locations (cat 3). (C) Classification accuracy between S1 firing rate responses to different stimulation pulse-rates (synchronous stimulation on all 16 DRG electrodes, amplitude = 6 μA; cat 2). The color scale for classification accuracy is shown at the bottom left. The inset shows examples of PSTH plots for one S1 channel for a range of stimulation pulse-rates; plots show the mean +/− 1 SEM firing rates. Asterisks indicate significance ($p<0.001$).

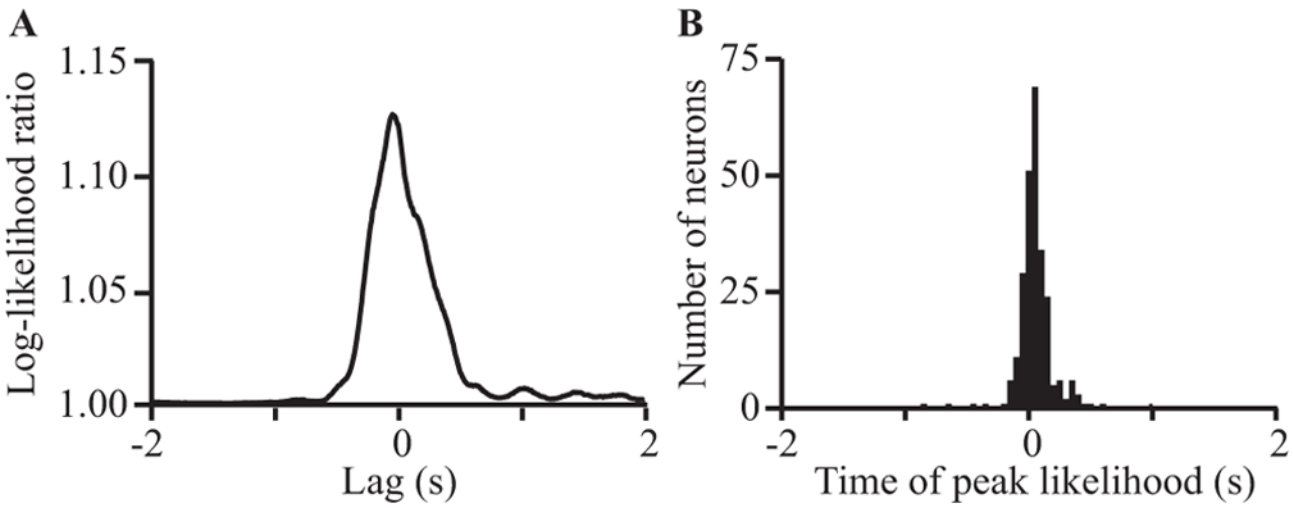

Fig. 6.

Log-likelihood ratio for GLM predictions from area 2 neurons recorded from monkeys. (A) shows a curve representing the log-likelihood ratio as a function of lag for a representative neuron. (B) shows the distribution of the times of the peak of the log-likelihood ratio curve for all cells that had a peak at least twice the variance over the full range of lags (± 5 seconds). The dependent axis is configured such that negative lag implies neural activity before movement (motor-like) and positive lag implies neural activity after movement (sensory-like).

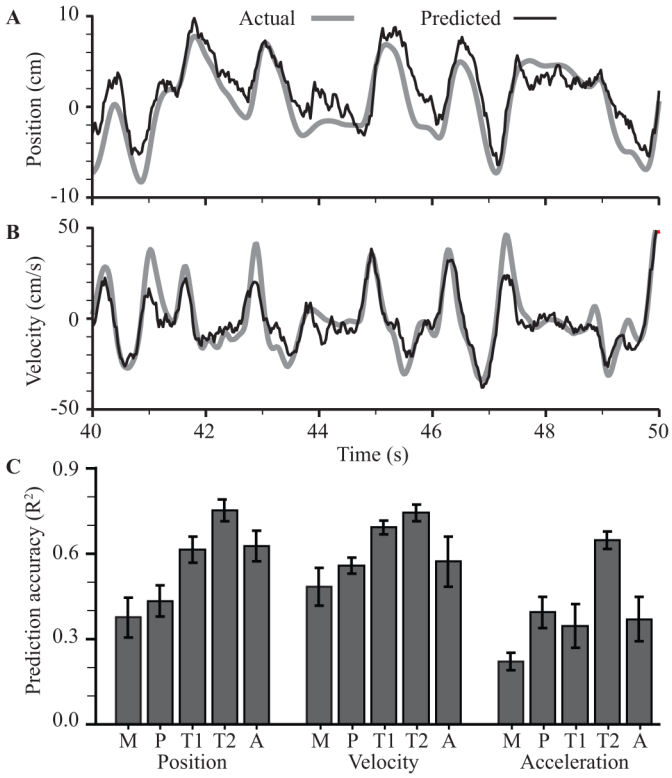

Fig. 7.

Decoding of kinematics from neural activity recorded from area 2 in monkeys. Actual (solid) and predicted (dashed) horizontal position (A) and velocity (B) are shown for a representative ten second span from one of the sessions. (C) Goodness of fit for predictions of limb endpoint kinematics from each array. Shown are R^2 values position, velocity, and acceleration calculated on 10-fold cross-validated data presented as mean +/- standard deviation across folds. Predictions from monkey M's array consistently underperformed the others for unknown reasons.

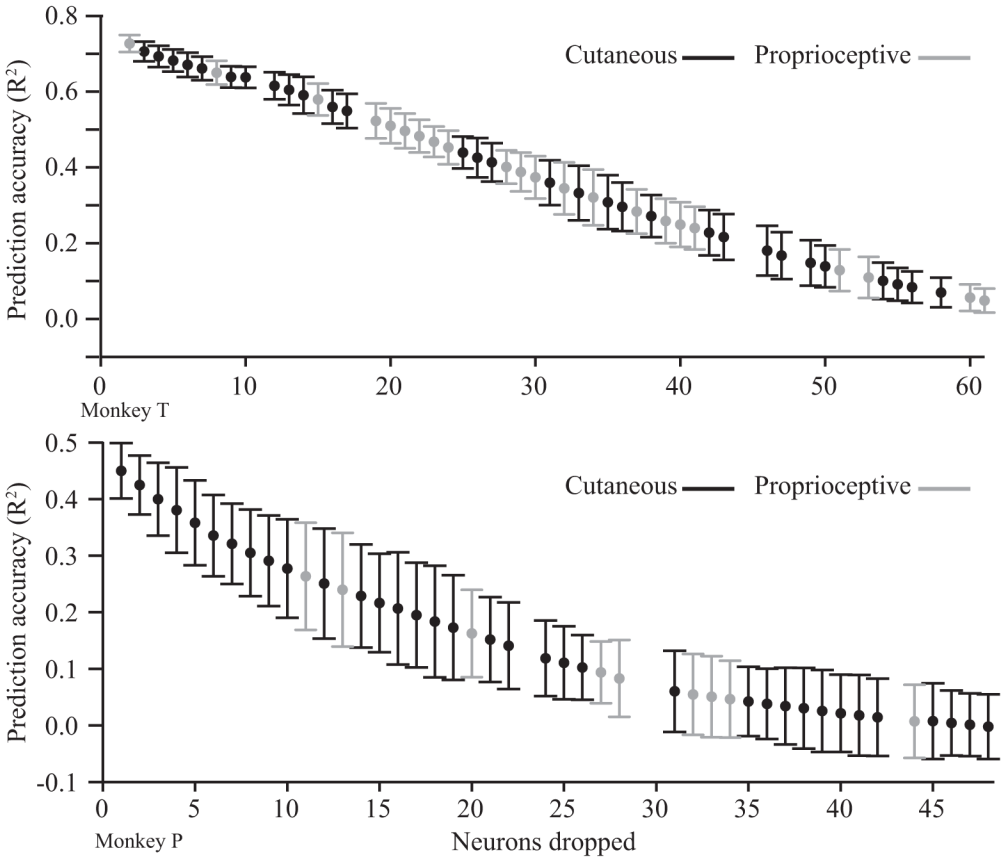

Fig. 8.

Velocity prediction accuracy while dropping the most uniquely informative neurons for two monkeys. Steps on which a neuron with a proprioceptive RF was dropped are shown in gray, cutaneous in black. The intermingling of gray and black bars indicates that neurons with proprioceptive RFs were not more informative about kinematics than neurons with cutaneous RFs.

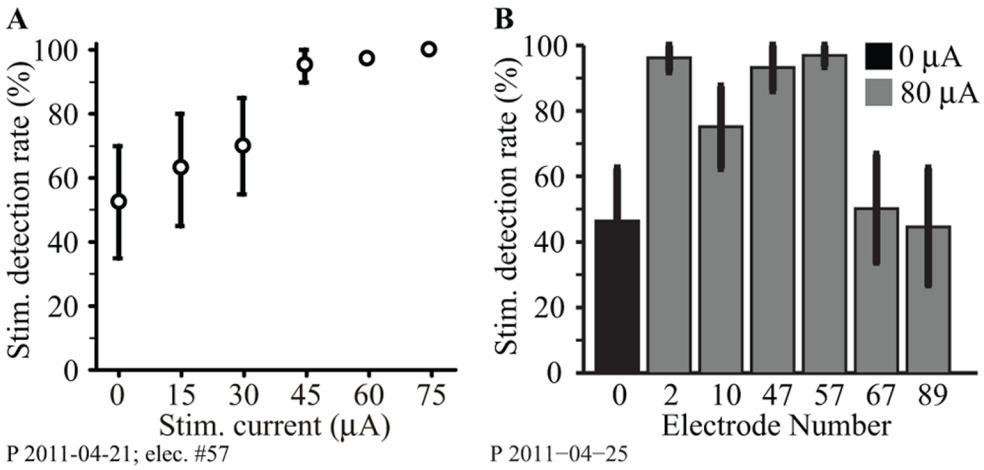

Fig. 9.

Area 2 ICMS detection results for monkey P. (A) ICMS detection rates for single-electrode stimulation across a range of currents. (B) Response percentage for 6 different electrodes, each stimulated individually at 80 μA, in another experimental session (gray bars). Black bar indicates the condition in which no stimulation was delivered.